Prominent phonon transmission across aperiodic superlattice through coherent

mode-conversion

Theodore Maranets¹ and Yan Wang¹

Department of Mechanical Engineering, University of Nevada, Reno, Reno, NV, 89557,

USA

(*Electronic mail: tmaranets@unr.edu)

In both particle and wave descriptions of phonons, the dense, aperiodically arranged inter-

faces in aperiodic superlattices are expected to strongly attenuate thermal transport due to

phonon-interface scattering or broken long-range coherence. However, non-trivial thermal

conductivity is still observed in these structures. In this study, we reveal that incoher-

ent modes propagating in the aperiodic superlattice can convert, through interference, into

coherent modes defined by an approximate dispersion relation. This conversion leads to

high transmission across the aperiodic superlattice structure, which contains hundreds of

interfaces, ultimately resulting in non-trivial thermal conductivity. Such incoherent-to-

coherent mode-conversion behavior is extensively observed in periodic superlattices. This

work suggests an effective strategy to manipulate the phonon dispersion relation through

layer patterning or material choice, enabling precise control of phonon transmission across

aperiodic superlattices.

1

Superlattices (SLs), which are metamaterials composed of alternating layers of two or more materials, exhibit secondary periodicity that results in unique thermophysical properties ^{1–4}. These properties enable various novel applications, including quantum cascade lasers and thermoelectric materials ^{4–6}. The densely packed interfaces within SLs can induce significant phonon-interface scattering. Moreover, strong interference of scattered phonons manifest as wave-like phonons that propagate through the interfaces coherently without scattering ^{2,3,7,8}. A rigorous understanding of coherent phonon transport in SLs is of both fundamental significance for comprehending phonon behavior in complex materials and practical importance for thermal management in modern devices utilizing SL structures.

Recently, the disruption of the secondary periodicity in SLs has garnered significant attention due to its effectiveness in substantially reducing the lattice thermal conductivity of otherwise periodic SLs^{9–12}. Disrupted phonon coherence and destructive interference, particularly Anderson localization, are hypothesized to be the primary mechanisms, supported by extensive yet mostly indirect evidence from spectral phonon analysis and length-dependent thermal conductivity data obtained from atomistic simulations^{9,10,13}. Furthermore, it has been demonstrated that the lattice thermal conductivity of well-randomized SLs can be lower than that of random alloys^{10,14}. Ultimately, achieving full-spectrum suppression of phonon transmission across aperiodic SLs to attain the lowest possible lattice thermal conductivity is desirable. Recent studies employing machine learning have optimized the layer thicknesses of aperiodic SLs to minimize thermal conductivity, though the precise phonon mechanisms responsible for this minimized conductivity remain elusive^{11,15–17}.

In this study, we aim to address two fundamental questions regarding phonon transport in aperiodic SLs, which are characterized by aperiodically arranged interfaces between two distinct materials. First, we will examine the behavior of incoherent phonon modes that adhere to the phonon dispersion relations of the SL's base material. It is anticipated that these modes would experience scattering at the densely packed interfaces within the aperiodic SL, leading to diminished transmission across the device. However, the validity of this assumption remains to be thoroughly investigated. Both limited experimental data and modeling suggest that aperiodic SLs, even those optimized through machine learning algorithms, still exhibit non-trivial thermal conductivity, which suggests the existence of extended phonon modes that can readily transport across the aperiodic device ^{9–12,15,18}. Second, we seek to determine whether incoherent modes retain their original form or undergo conversion into new modes corresponding to the aperiodic SL structure as

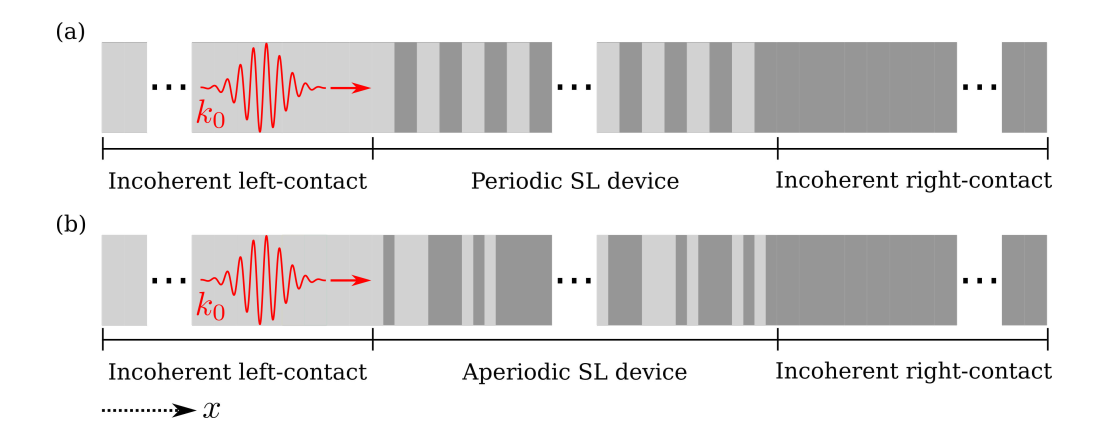


FIG. 1. Schematic illustrations of the simulation domain with periodic (a) and aperiodic SL (b) devices. The incident LA-mode incoherent phonon wave-packet centered at wavevector k_0 in reciprocal-space is generated in the left-contact and allowed to propagate into the device. The total energies of the left- and right-contacts, as well as the device are monitored throughout the simulation to compute the transmission across the device. Note: the illustrated sizes of the wave-packet and wavelength are not to scale.

a result of complex interference events at the interfaces. While previous studies have hypothesized such mode-conversion, direct evidence supporting this hypothesis is currently lacking ^{19–23}.

Atomistic phonon wave-packet simulations provide a direct means of analyzing phonon wave dynamics, with the ability to resolve mode, wavevector, and spatial coherence length^{20,24,25}. This allows for a rigorous examination of phonon scattering by specific heterogeneous structures, making the method particularly useful for investigating fundamental transport physics in metamaterials with complex structures. The technique employed in this study is adapted from the method developed by Schelling et al.²⁴. We utilize the same system configuration as in our previous work²³ as the model device. However, distinct from Ref. 23, in this study, we simulate a mode derived from the dispersion relation of one of the constituent materials (Fig. S1a) of the SL, as opposed to a mode derived from the SL's dispersion relation (Fig. S1b) as used in Ref. 23. We refer to these two distinct types of phonons modes as incoherent and coherent phonon modes, respectively. Coherent phonons obeying the SL dispersion are not to be confused with large coherence time, so called "coherent", modes produced by femtosecond laser pulses²⁶. The left- and right-contacts in the simulation domain consist of two pure materials in this study, in contrast to the periodic SL contacts used in Ref. 23. Additionally, unlike coherent modes, which can transmit across their corresponding SL devices without scattering, the incoherent phonon modes studied here exhibit significant scattering at the interfaces of both periodic and aperiodic SL devices (Figs. 1a and 1b,

respectively), resulting in non-unity transmission.

A phonon wave-packet is described by the following equation for atom displacement:

$$u_{i,n} = \frac{A_i}{\sqrt{m_i}} \varepsilon_{k_0,i} \exp\left(i[k_0 \cdot (x_n - x_0) - \omega_0 t]\right) \exp\left(-4(x_n - x_0 - v_{g0}t)^2 / l_c^2\right)$$
(1)

where $\varepsilon_{k_0,i}$, ω_0 , and v_{g0} are the associated eigenvector, frequency, and group velocity, respectively for the phonon centered at wavevector k_0 in reciprocal-space. A_i is the wave amplitude, m_i is the mass of atom i, x_n is the position of the nth unit cell containing atom i, x_0 is the initial position of the wave-packet, and l_c is the spatial coherence length. The wave-packet is generated by setting the real parts of Eqn. 1 and the time-derivative of Eqn. 1 evaluated at time t=0 as the initial atom displacement and velocity, respectively. A sufficiently large coherence length allows the wave-packet simulations to better capture any interference effects induced by the specific aperiodic SL structure, as revealed in our previous work²³. Specifically, we demonstrated that interference is weakened if the coherence length is not long enough, while use of a coherence length of four times the device length is sufficient. Other parameters such as the boundary conditions, size of the device, cross-sectional area, and transmission calculation are the same as Ref. 23. The simulations are performed using the LAMMPS package²⁷.

In Figs. 2a and 2b, we present the transmission of the longitudinal-acoustic (LA) incoherent phonon wave-packet through the periodic and aperiodic SL devices, respectively. The near-unity phonon transmission in the long-wavelength (or small-wavevector) limit of both figures is due to the wavelengths being significantly larger than the period thicknesses, and thus minimally affected by the interfaces^{23,28–30}. The periodic SL spectrum exhibits an oscillatory pattern of near-unity and zero transmission values, with the highest transmission occurring at the longest wavelengths and a slightly decreasing trend as the wavelength shortens. In contrast, the aperiodic SL spectrum shows strong transmission at the long-wavelength limit, while the remainder of the spectrum is flattened at zero, except for a narrow but prominent transmission peak at an intermediate wavelength.

We emphasize the prominent transmission of intermediate-wavelength (1.5 to 2 nm) incoherent phonons across the aperiodic SL (Fig. 2b) is quite surprising, regardless of whether the phonons are treated as particle-like or wave-like. Considering the multitude and density of interfaces in both periodic and aperiodic SLs, particle-like phonons are not expected to strongly transmit through the devices due to severe interface scattering. Specifically, considering that there are 256 interfaces in our device, the overall transmission across the entire device would be on the order of τ^{256} , which gives a nearly zero transmission on the order of 10^{-6} even if the transmission coefficient

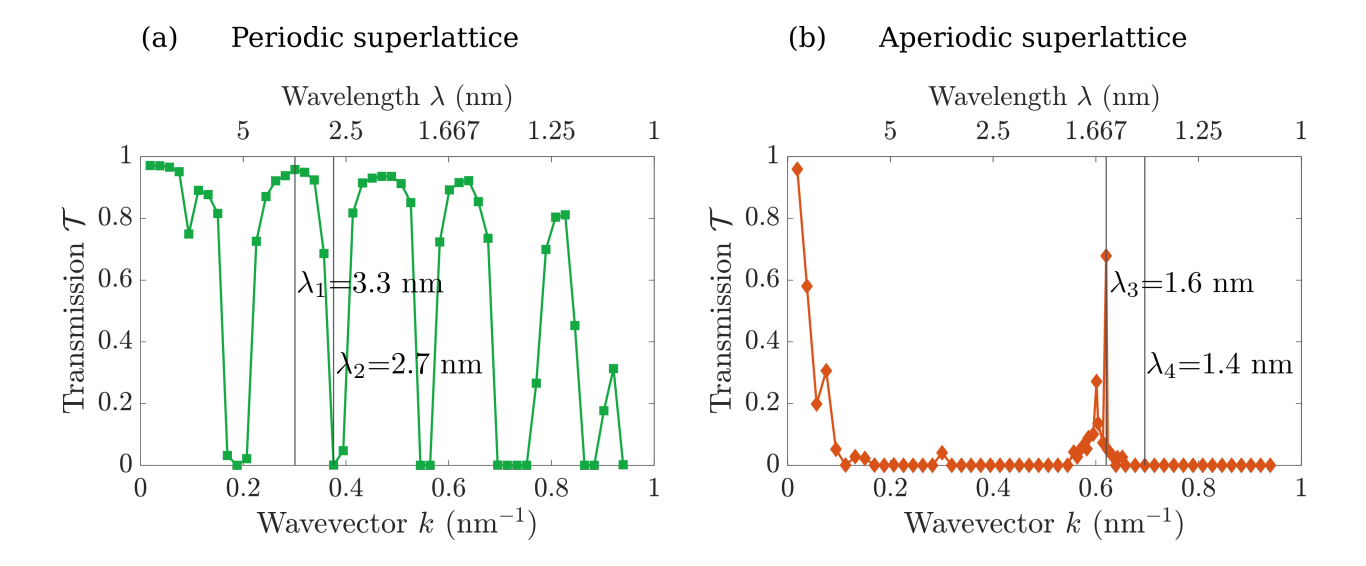


FIG. 2. Transmission \mathscr{T} versus wavevector k (or inverse of wavelength λ) for the LA-mode incoherent phonon wave-packet propagating through the periodic (a) and aperiodic SL (b) devices as illustrated in Figs. 1a and 1b, respectively. Key wavelengths $\lambda_1 = 3.3$ nm, $\lambda_2 = 2.7$ nm, $\lambda_3 = 1.6$ nm, and $\lambda_4 = 1.4$ nm analyzed in this letter are indicated in the figures by the vertical black lines. Only the frequencies below the cutoff frequency of the two constituent layer materials of the SL are studied.

for each individual interface τ is as high as 0.95. For wave-like phonons, the lack of a periodicity in aperiodic SLs means there is no extended phonon modes in the structure, so we should also expect significant interface scatterings that lead to low transmission across the device, like (though not as low as) the particle-like case above.

To elucidate the prominent transmission peak in the aperiodic SL case, we first focus on understanding the transmission values in the periodic SL. The locations of the transmission dips in Fig. 2a closely match previous first-principles analyses of Bragg reflection of phonons in the cross-plane direction of the periodic SL^{31–33} as well as phonon-imaging experiments^{34,35}. When the Bragg scattering condition is met, the interference of phonon waves results in total reflection, attenuating energy transport and producing band gaps in the center and edges of the periodic SL Brillouin zone. Conversely, the high transmission of incoherent modes in a periodic SL is suggested to arise from mode-conversion (through interference) to coherent modes, which follow the periodic SL dispersion. Otherwise, the strong interface scattering of incoherent modes by the multiple layers in the device would result in nearly zero transmission across the SL.

To elucidate the mechanisms of transmission, we conduct several quantitative analyses of the wave dynamics. In Fig. 3, we present the plots of atom velocity versus real-space position and

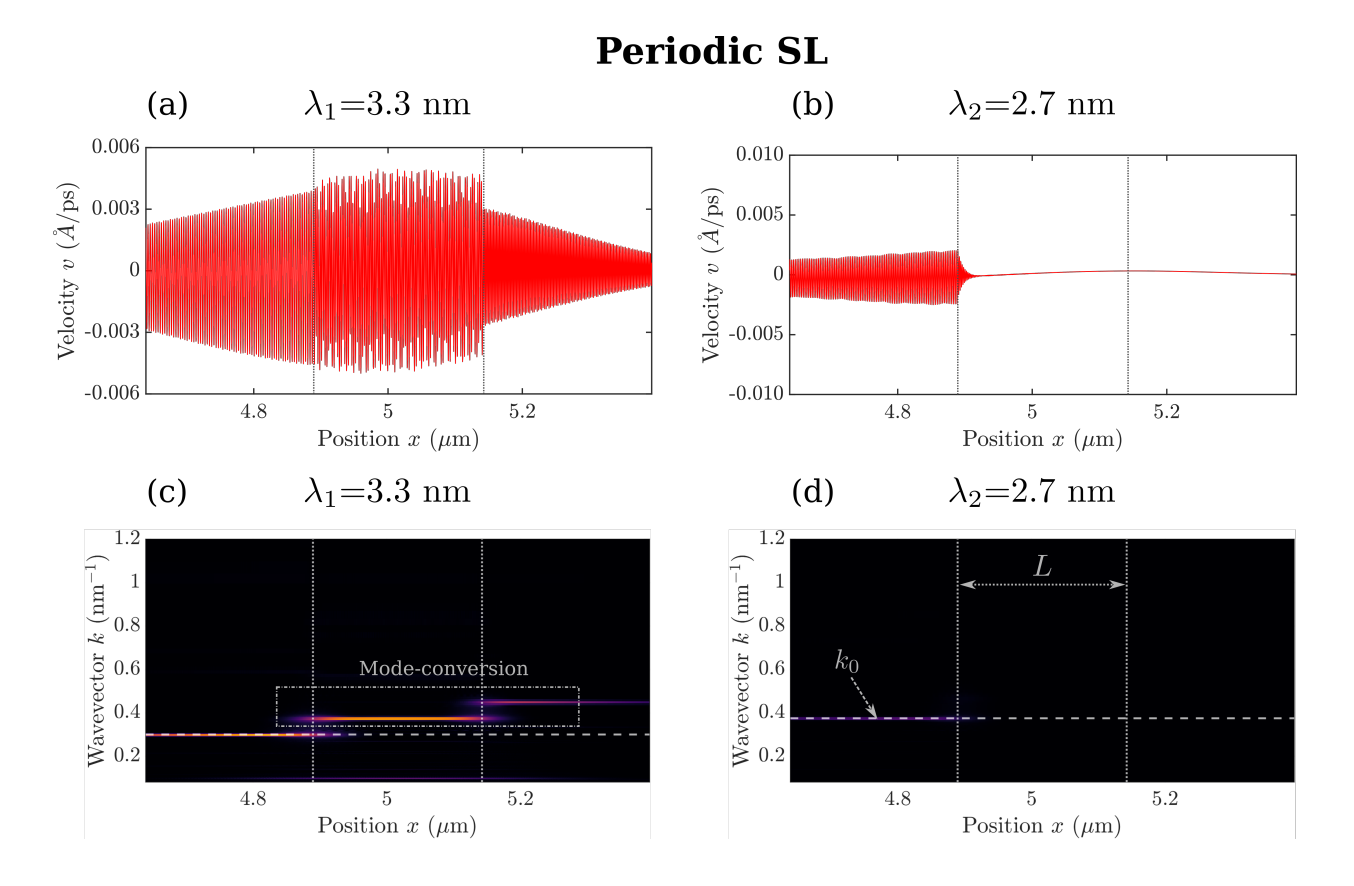


FIG. 3. Snapshots of the atom velocity versus real-space position when the wave-packet scatters through the periodic SL device for wavelengths $\lambda_1 = 3.3$ nm (a) and $\lambda_2 = 2.7$ nm (b), representative cases of near-unity and zero transmission as shown in Fig. 2a, respectively. Snapshots of the reciprocal-space wavelet transform when the wave-packet scatters through the periodic SL device for wavelengths λ_1 (c) and λ_2 (d). The dotted vertical lines denote the position and thickness L of the device. The dashed horizontal line denotes the central wavevector k_0 of the incident wave-packet. Illuminated regions in the heat map not centered about the k_0 line indicate mode-conversion.

the reciprocal-space wavelet transform³⁶ for two wavelengths marked in Fig. 2a, λ_1 and λ_2 , representative cases of near-unity and zero transmission in the periodic SL, respectively. Examining Figs. 3a and 3c, we find that high transmission is associated with the incident incoherent phonon wave-packet mode-converting inside the periodic SL device. Similarly, the zero transmission of λ_2 is owed to the incoherent mode not mode-converting as seen in Figs. 3b and 3d.

We repeat these analyses for the aperiodic SL, focusing on two wavelengths marked in Fig. 2b: λ_3 (transmission peak) and λ_4 (zero transmission). Studying the velocity plots and wavelet transforms of the two wavelengths in Fig. 4, we observe that the prominent transmission of λ_3 (Figs. 4a

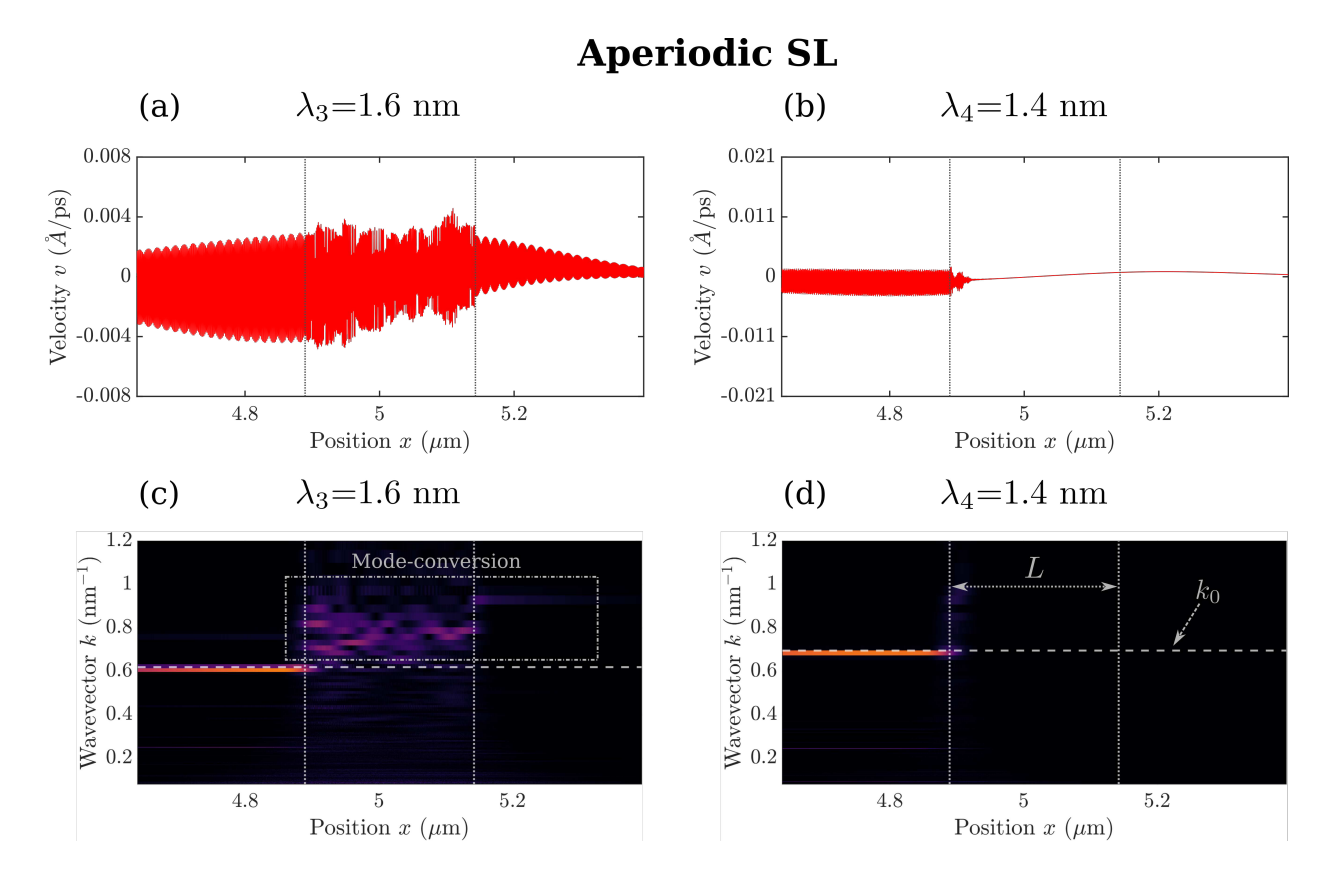


FIG. 4. Snapshots of the atom velocity versus real-space position when the wave-packet scatters through the aperiodic SL device for wavelengths $\lambda_3 = 1.6$ nm (a) and $\lambda_4 = 1.4$ nm (b), representative cases of the transmission peak and zero transmission as shown in Fig. 2b, respectively. Snapshots of the reciprocal-space wavelet transform when the wave-packet scatters through the aperiodic SL device for wavelengths λ_3 (c) and λ_4 (d). The dotted vertical lines denote the position and thickness L of the device. The dashed horizontal line denotes the central wavevector k_0 of the incident wave-packet. Illuminated regions in the heat map not centered about the k_0 line indicate mode-conversion.

and 4c) is a consequence of substantial mode-conversion. Likewise, the λ_4 phonon does not undergo mode-conversion, as shown in Figs. 4b and 4d.

To gain further insights into mode-conversion, we examine the vibrational spectra of both the periodic and aperiodic SL. The atomistic wave-packet simulation is approximately harmonic, making all scattering in the simulation elastic^{20,24,25}. For the periodic SL λ_1 phonon, plotting the mode-converted wavevector at the incident phonon frequency reveals that the mode-converted phonon exactly falls in the second Brillouin zone of the periodic SL dispersion relation (Fig. 5a), evidencing the manifestation of coherent modes obeying the dispersion relation of the periodic

SL through interference of incoherent phonons. Interference facilitates mode-conversion in the following way. Constructive interference promotes the transmission of phonons, particularly the incoherent phonons studied in this work, across multiple interfaces, allowing the phonons to extend over the superlattice, which includes both types of base materials. Such an extended phonon mode³⁷, or collective vibration of atoms at the same frequency across many superlattice layers, appears as a superlattice mode, so called coherent phonon, as shown in Fig. 5a.

In contrast to the periodic SL, the aperiodic SL lacks a well-defined phonon dispersion relation, rendering lattice dynamics unsuitable for its study. One approach to explore its vibrational spectrum is computing the spectral energy density through equilibrium molecular dynamics simulations³⁸. In Fig. 5b, we present the spectral energy density of the aperiodic SL below the Debye temperature. The mode-converted phonon in the λ_3 case falls on a somewhat faint band in the second Brillouin zone. This finding reveals that, akin to the periodic SL, the non-trivial thermal conductivity observed in the aperiodic SL device stems from incoherent phonons converting to coherent modes defined by an approximate dispersion relation. Consequently, the overall level of mode-conversion appears subject to how the specific layering structure affects interference states and thus dispersion.

In summary, through atomistic wave-packet simulations, we found a prominent transmission peak of incoherent phonons in the aperiodic SL; a surprising result considering the aperiodically arranged interfaces are expected to strongly scatter both particle-like and wave-like modes. The peak is owed to the mode-conversion of incoherent phonons to coherent modes defined by the approximate dispersion relation of the aperiodic SL. This behavior is similarly observed in the periodic SL where non-Bragg-reflected phonons can convert to coherent modes from the periodic SL dispersion relation and thus exhibit near-unity transmission. In both the periodic and aperiodic SL, the mode-converted phonons are found to lie outside the first Brillouin zone. Our results reveal that phonon transmission in both the periodic and aperiodic SL is dictated by the degree to which incoherent modes can convert to coherent modes defined by the device's phonon dispersion relation. From this, we infer that manipulating the dispersion relation of the SL through changes in the layering pattern is a pathway to tailoring thermal conductivity to specific limits, depending on the application.

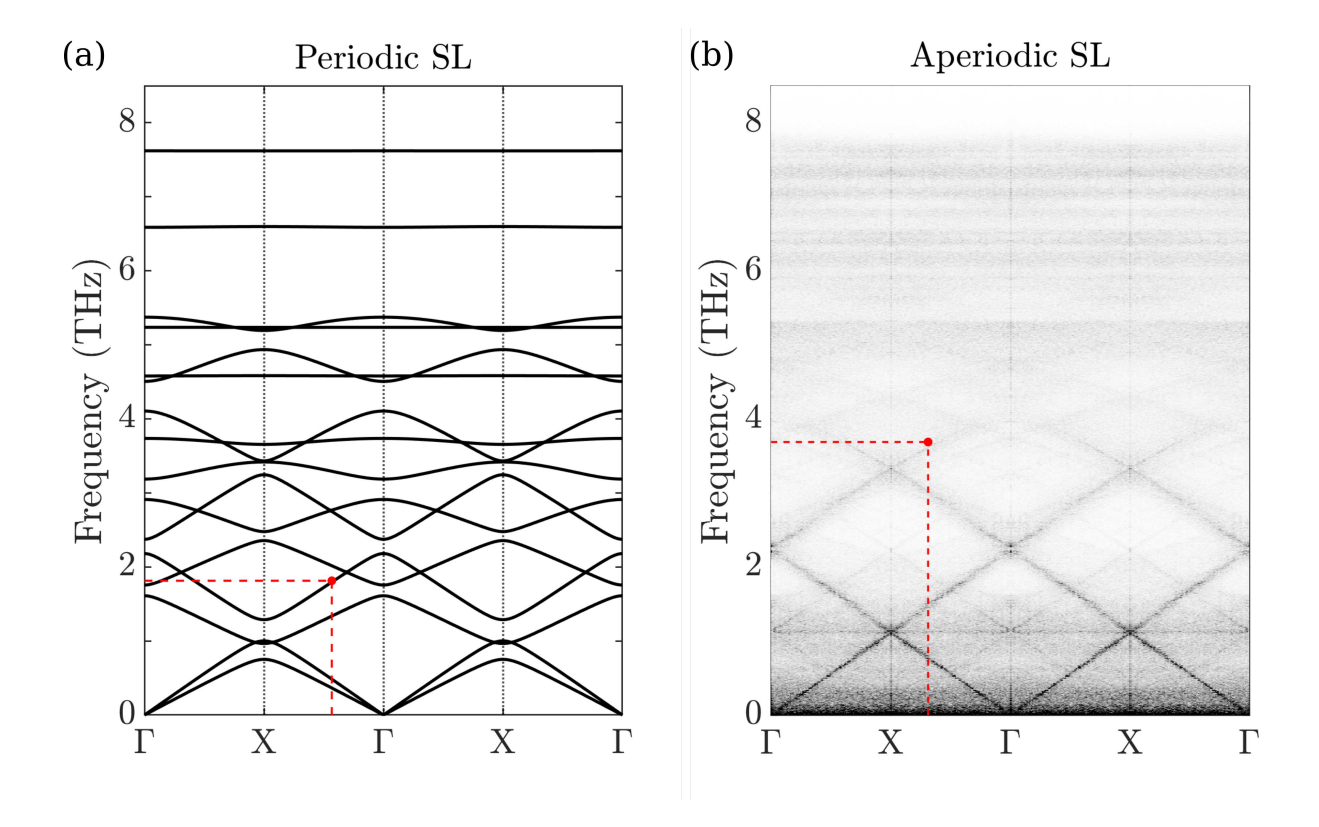


FIG. 5. (a) Phonon dispersion relation of the periodic SL with the mode-converted phonon in the $\lambda_1 = 3.3$ nm case (Fig. 3c) located with the red dot and dashed lines. (b) Spectral energy density heat map of the aperiodic SL with the mode-converted phonon in the $\lambda_3 = 1.6$ nm case (Fig. 4c) located with the red dot and dashed lines.

SUPPLEMENTARY MATERIAL

See the supplementary material for Figs. S1a and Fig S1b.

ACKNOWLEDGEMENTS

The authors thank the support from the Nuclear Regulatory Commission (award number: 31310021M0004) and the National Science Foundation (award number: 2047109). The authors also would like to acknowledge the support of Research and Innovation and the Cyberinfrastructure Team in the Office of Information Technology at the University of Nevada, Reno for facilitation and access to the Pronghorn High-Performance Computing Cluster.

AUTHOR DECLARATIONS

A. Conflict of Interest

The authors have no conflicts to disclose.

B. Author Contributions

Theodore Maranets: Writing – review & editing (equal), Writing – original draft (lead), Software (lead), Methodology (lead), Formal analysis (equal), Conceptualization (equal). **Yan Wang:** Writing – review & editing (equal), Writing – original draft (equal), Supervision (lead), Funding acquisition (lead), Formal analysis (equal), Conceptualization (equal).

DATA AVAILABILITY

The data that support the findings of this study are available from the corresponding author upon reasonable request.

REFERENCES

- ¹G. Xie, D. Ding, and G. Zhang, Advances in Physics: X **3**, 1480417 (2018).
- ²R. Anufriev, J. Maire, and M. Nomura, APL Materials **9** (2021).
- ³Z. Zhang, Y. Guo, M. Bescond, J. Chen, M. Nomura, and S. Volz, APL Materials 9 (2021).
- ⁴X. Qian, J. Zhou, and G. Chen, Nature Materials **20**, 1188 (2021).
- ⁵L. Shi, C. Dames, J. R. Lukes, P. Reddy, J. Duda, D. G. Cahill, J. Lee, A. Marconnet, K. E. Goodson, J.-H. Bahk, *et al.*, Nanoscale and Microscale Thermophysical Engineering **19**, 127 (2015).
- ⁶S. Volz, J. Ordonez-Miranda, A. Shchepetov, M. Prunnila, J. Ahopelto, T. Pezeril, G. Vaudel, V. Gusev, P. Ruello, E. M. Weig, *et al.*, The European Physical Journal B **89**, 1 (2016).
- ⁷M. Maldovan, Nature materials **14**, 667 (2015).
- ⁸R. Hu and X. Luo, National Science Review **6**, 1071 (2019).
- ⁹Y. Wang, H. Huang, and X. Ruan, Physical Review B **90**, 165406 (2014).
- ¹⁰Y. Wang, C. Gu, and X. Ruan, Applied Physics Letters **106** (2015).

- ¹¹P. Chakraborty, Y. Liu, T. Ma, X. Guo, L. Cao, R. Hu, and Y. Wang, ACS applied materials & interfaces **12**, 8795 (2020).
- ¹²P. Chakraborty, I. A. Chiu, T. Ma, and Y. Wang, Nanotechnology **32**, 065401 (2020).
- ¹³T. Ma, C.-T. Lin, and Y. Wang, 2D Materials **7**, 035029 (2020).
- ¹⁴P. Chakraborty, L. Cao, and Y. Wang, Scientific reports 7, 8134 (2017).
- ¹⁵P. R. Chowdhury, C. Reynolds, A. Garrett, T. Feng, S. P. Adiga, and X. Ruan, Nano Energy **69**, 104428 (2020).
- ¹⁶R. Hu, S. Iwamoto, L. Feng, S. Ju, S. Hu, M. Ohnishi, N. Nagai, K. Hirakawa, and J. Shiomi, Physical Review X **10**, 021050 (2020).
- ¹⁷H. Wei, H. Bao, and X. Ruan, Energy and AI **8**, 100153 (2022).
- ¹⁸Y. Liu, R. Hu, Y. Wang, J. Ma, Z. Yang, and X. Luo, Energy and AI **3**, 100046 (2021).
- ¹⁹S.-i. Tamura and F. Nori, Physical Review B **41**, 7941 (1990).
- ²⁰P. Schelling and S. Phillpot, Journal of Applied Physics **93**, 5377 (2003).
- ²¹P. Jiang, Y. Ouyang, W. Ren, C. Yu, J. He, and J. Chen, APL Materials 9 (2021).
- ²²T. Ma and Y. Wang, Materials Today Physics **29**, 100884 (2022).
- ²³T. Maranets, M. Nasiri, and Y. Wang, Physics Letters A, 129572 (2024).
- ²⁴P. K. Schelling, S. R. Phillpot, and P. Keblinski, Applied Physics Letters **80**, 2484 (2002).
- ²⁵P. Schelling, S. Phillpot, and P. Keblinski, Journal of Applied Physics **95**, 6082 (2004).
- ²⁶B. Rethfeld, K. Sokolowski-Tinten, D. Von Der Linde, and S. I. Anisimov, Applied Physics A **79**, 767 (2004).
- ²⁷A. P. Thompson, H. M. Aktulga, R. Berger, D. S. Bolintineanu, W. M. Brown, P. S. Crozier, P. J. In't Veld, A. Kohlmeyer, S. G. Moore, T. D. Nguyen, *et al.*, Computer Physics Communications **271**, 108171 (2022).
- ²⁸B. Latour, S. Volz, and Y. Chalopin, Physical Review B **90**, 014307 (2014).
- ²⁹H. R. Seyf and A. Henry, Journal of Applied Physics **120** (2016).
- ³⁰B. Latour and Y. Chalopin, Physical Review B **95**, 214310 (2017).
- ³¹S. Tamura, D. Hurley, and J. Wolfe, Physical Review B **38**, 1427 (1988).
- ³²S. Tamura and J. Wolfe, Physical Review B **38**, 5610 (1988).
- ³³S.-i. Tamura, Physical Review B **39**, 1261 (1989).
- ³⁴D. Hurley, S. Tamura, J. Wolfe, and H. Morkoc, Physical review letters **58**, 2446 (1987).
- ³⁵Y. Tanaka, M. Narita, and S.-i. Tamura, Journal of Physics: Condensed Matter **10**, 8787 (1998).
- ³⁶C. H. Baker, D. A. Jordan, and P. M. Norris, Physical Review B **86**, 104306 (2012).

³⁷K. Kothari and M. Maldovan, Nanoscale and Microscale Thermophysical Engineering **22**, 239 (2018).

³⁸J. A. Thomas, J. E. Turney, R. M. Iutzi, C. H. Amon, and A. J. McGaughey, Physical Review B **81**, 081411 (2010).